Electron momentum relaxation time and mobility in a free-standing quantum well

N. A. Bannov,[a] V. A. Aristov, and V. V. Mitin
Department of Electrical and Computer Engineering, Wayne State University, Detroit, Michigan 48202

(Received 22 March 1995; accepted for publication 29 June 1995)

Kinetic characteristics of the electron transport in a free-standing quantum well are studied theoretically. The quantization of acoustic phonons in a free-standing quantum well is taken into account and electron interactions with confined acoustic phonons through the deformation potential are treated rigorously. The kinetic equation for the electron distribution function is solved numerically for nondegenerate as well as degenerate electron gases and the electron momentum relaxation time and the electron mobility are obtained. At high lattice temperatures the electron momentum relaxation time is very similar to that obtained in the test particle approximation. Its dependence on the electron energy has steps which occur at the threshold energies for the dilatational phonons because an additional electron scattering by the corresponding acoustic phonon becomes important. The first mode makes the main contribution to the electron scattering, the contributions of the zeroth and the second modes are also important, the third and the higher modes practically unnoticeable for the studied electron concentrations and quantum well width. At lattice temperatures lower than the energy of the first dilatational acoustic mode the electron momentum relaxation time dependence on energy has additional peaks (in comparison with the test particle approximation) associated with electron scattering by several lowest acoustic phonon modes. These peaks occur near the Fermi energy in the degenerate case and in the energy range of the first dilatational modes in the nondegenerate case. They are especially pronounced for the degenerate electron gas. The temperature dependence of the electron mobility is similar to that described by the Bloch-Grüneisen formula, however we obtained a smaller negative exponent in the low temperature region.

I. INTRODUCTION

At present there is a considerable interest toward new type of nanostructures: free-standing quantum wells (FSQWs) and free-standing quantum wires (FSQWIs). These structures are either solid plates and rods connected to the semiconductor substrate by the side of the smallest cross-section or thin films and bars supported on their ends. They may be fabricated by various etching and lithographic techniques or by metal-organic epitaxy[1–7] (see additional references in review[1]). There are several possible applications of the free-standing structures. They may be used for probing of the local properties of solids and there are several works where such possibilities have been demonstrated.[6] Free-standing quantum structures may find applications as very sensitive sensors of forces or displacements in ways similar to those used for thin film sensors.[8] There exists a variety of potential uses of free-standing structures for electronic and photonic applications, e.g., as low voltage field emitters, light emitting devices, mirrors for optical resonators.[1,5,9,10]

A very important peculiarity of free-standing structures is the quantization of acoustic phonons. It occures due to the transverse resonance of the acoustic waves just as it occur for the electromagnetic waves in waveguides where an integer number of half-wavelengths should fit between boundaries. However in the case of acoustic waves the rules for quantization are more complicated because the transverse resonance conditions should be satisfied simultaneously for both longitudinal and transverse waves. The quantization of acoustic waves results in the occurrence of several acoustic phonon branches with different frequencies. The acoustic phonon quantization has been observed both in optical and electrical experiments.[6,11] There are only a few papers devoted to a theoretical study of transport properties of the charge carriers in free-standing structures where the electron interactions with acoustic phonons through the deformation potential are of great importance.[12–18] In Refs. 12 and 14 the Hamiltonians for electron interactions with confined acoustic phonons in FSQWs have been obtained and the electron scattering rate and the momentum and energy relaxation times have been analyzed in the test particle approximation. A similar approach has been used in Ref. 15 to study the electron scattering rate in FSQWIs. The electron heating in thin metal films and wires has been studied both theoretically[18] and experimentally.[11]

In this paper we have investigated the electron transport in FSQWs allowing for the exact form of the confined acoustic modes and their spectrum. We have solved the kinetic equation for electrons in the low electric field limit, obtained the electron distribution function, the momentum relaxation time, and the electron mobility, and have analyzed their temperature dependences. In the next section we will formulate the problem mathematically, give the formulae for dilatational modes and the equations for the electron–phonon interactions, and discuss the expressions for scattering rates. Then we will consider the kinetic equation describing the electron transport in FSQW, transform it to the form of the integral equation for to the momentum relaxation rate, and

[a]Electronic mail: bannov@ciao.eng.wayne.edu

 0021-8979/95/78(9)/5503/8/$6.00

discuss the numerical solution of the integral equation and the physical interpretation of the obtained results in terms of individual scattering events. The last section of the paper is devoted to the analysis of the low field electron mobility.

II. ELECTRON INTERACTIONS WITH CONFINED ACOUSTIC PHONONS THROUGH THE DEFORMATION POTENTIAL

This section is aimed at deriving a formula for the "generalized" scattering rate [given by Eqs. (8)] which takes into account peculiarities of electron scatterings by acoustic phonons in FSQWs. We will start with consideration of the acoustic modes in FSQWs neglecting the distorsions of the acoustic vibrations which result from the contact with a solid substrate. We assume that the solid slab is infinite. The acoustic modes may be determined by solving the eigenvalue problem for elastodynamic equations (see, e.g., Ref. 19). We will use a coordinate system such that axis z is perpendicular to the semiconductor slab, and FSQW is bounded by the planes $z=-a/2$ and $z=+a/2$, where a is the width of the quantum well. The boundary conditions for the eigenvalue problem state that the $z-$components of the stress tensor are equal to zero at the boundaries of the slab. These conditions correspond to free (unstressed) surfaces of the slab. The specified boundary conditions result in coupling of longitudinal and transverse acoustic waves; so eigenmodes represent, generally speaking, a mixture of both longitudinal and transverse waves.

There are three different types of acoustic modes in FSQWs: shear waves, dilatational waves and the flexural waves (see e.g., Refs. 12 and 19 and references therein). They differ by their specific symmetry. The shear phonons do not interact with electrons through the deformation potential because they are completely transverse. We restrict our consideration by the extreme quantum limit where only the first electron subband is occupied and we assume that electron potential energy is a symmetric function in respect to the mid-plane. Under these conditions only the dilatational acoustic phonons contribute to the electron scattering through the deformation potential, while interactions with flexural acoustic phonons is forbidden by the selection rules originated from the symmetry of the electron and phonon wave functions.[12,14]

The dilatational phonons are characterized by the in-plane wave-vector, $\mathbf{q}_\parallel$, mode number, n ($n=0,1,2,3,\ldots$), and the phonon frequency, $\omega_n(\mathbf{q}_\parallel)$. We would like to emphasize that the lowest dilatational phonon mode is the zeroth mode, the next mode is the first mode, and so on. For the sake of simplicity we will direct the axis x along the vector $\mathbf{q}_\parallel$, so it has coordinates $\mathbf{q}_\parallel=(q_x,0)$.

The Hamiltonian for electron interactions with dilatational phonons has the following form[12,14]

$$H_{def}=\sum_{\mathbf{q}_\parallel,n} e^{i\mathbf{q}_\parallel\mathbf{r}_\parallel}\Gamma_d(\mathbf{q}_\parallel,n,z)[c_n(\mathbf{q}_\parallel)+c_n^\dagger(-\mathbf{q}_\parallel)], \tag{1}$$

where

$$\Gamma_d(\mathbf{q}_\parallel,n,z)=F_{d,n}\sqrt{\frac{\hbar E_a^2}{2\mathscr{A}\rho\omega_n(\mathbf{q}_\parallel)}}\left[(q_{t,n}^2-q_x^2)\times(q_{l,n}^2+q_x^2)\sin\left(\frac{aq_{t,n}}{2}\right)\cos(q_{l,n}z)\right], \tag{2}$$

$c_n(\mathbf{q}_\parallel)$ and $c_n^\dagger(\mathbf{q}_\parallel)$ are the phonon annihilation and creation operators, $F_{d,n}$ is the dilatational mode normalization constant, E_a is the deformation potential constant, ρ is the density, $\mathscr{A}$ is the area of the slab, $q_{t,n}=q_{t,n}(q_x)$ and $q_{l,n}=q_{l,n}(q_x)$ are the parameters obtained from the solution of the system of dispersion equations.[14] The normalization constants, $F_{d,n}$, are determined from the mode normalization conditions

$$|F_{d,n}|^2\int_{-a/2}^{a/2}[u_x^*(\mathbf{q}_\parallel,n,z)u_x(\mathbf{q}_\parallel,m,z)+u_z^*(\mathbf{q}_\parallel,n,z)u_z(\mathbf{q}_\parallel,m,z)]dz=\delta_{n,m},$$

where $\delta_{n,m}$ is the Kronecker delta, u_x,u_z are the $x-$ and $z-$ components of the vector of relative displacements, which for the case of dilatational modes have the following form

$$u_x=iq_x\left[(q_x^2-q_t^2)\sin\frac{q_ta}{2}\cos q_lz+2q_lq_t\sin\frac{q_la}{2}\cos q_tz\right], \tag{3}$$

$$u_z=q_l\left[-(q_x^2-q_t^2)\sin\frac{q_ta}{2}\sin q_lz+2q_x^2\sin\frac{q_la}{2}\sin q_tz\right]. \tag{4}$$

We have omitted the subscript n in the notations for q_l and q_t to simplify Eqs. (3) and (4). The y component of the vector of relative displacement vanishes in the specified coordinate system. The parameters $q_{l,n}$ and $q_{t,n}$ play role of the z components of the phonon wave vector for dilatational modes. These functions, $q_{t,n}=q_{t,n}(q_x)$, $q_{l,n}=q_{l,n}(q_x)$, and the phonon frequency, $\omega_n(\mathbf{q}_\parallel)$, calculated numerically for GaAs FSQW of width 100 Å are shown in Fig. 1. The values of q_t and q_l above the abscissa are real and below the abscissa are pure imaginary. If the parameter q_l or both the parameters q_l and q_t are pure imaginary numbers, the dilatational mode has either partially or completely surface bound character in accordance with Eqs. (3) and (4). However, the spatial dependence of the the Hamiltonian for electron interactions with dilatational phonons is determined only by the parameter q_l [see Eq. (2)]. Accordingly, if q_l is a pure imaginary number, the electron interaction with the appropriate phonon will be suppressed.

The electron probability density for the transition from initial state $\mathbf{k}_\parallel$ to the final state $\mathbf{k}_\parallel'$ due to an interaction with the dilatational phonon of mode m and in-plane wave vector $\mathbf{q}_\parallel$ may be determined from the Fermi golden rule. This probability density is given by the formula

$$W_{\mathbf{k}_\parallel\to\mathbf{k}_\parallel'}^{\{ab\}_{em}}=\frac{\pi E_a^2}{\mathscr{A}\rho}\mathscr{F}^{\{ab\}_{em}}(m,q_\parallel)\,\delta_{\mathbf{k}_\parallel\pm\mathbf{q}_\parallel,\mathbf{k}_\parallel'}\delta[\varepsilon\pm\hbar\omega_m(\mathbf{q}_\parallel)-\varepsilon'], \tag{5}$$

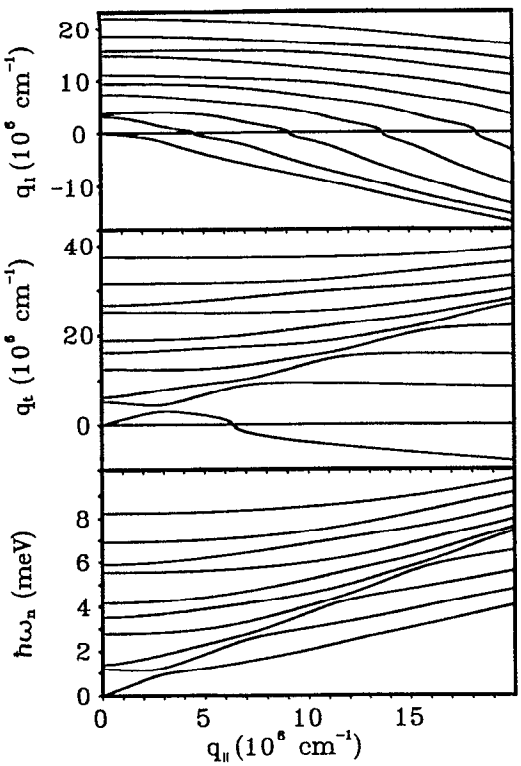

FIG. 1. Parameters q_l and q_t and phonon frequency ω_n as functions of in-plane wave vector, q_x, for the 10 lowest dilatational modes. The values of q_l and q_t above the abscissa are real, the values of q_l and q_t below the abscissa are pure imaginary.

where

$$\mathscr{F}^{\{ab\}}_{\{em\}}(m,q_\parallel) = \frac{\left(n_{\mathbf{q}_\parallel,m}+\frac{1}{2}\mp\frac{1}{2}\right)|F_{d,m}|^2(q_{t,m}^2-q_x^2)^2(q_{l,m}^2+q_x^2)^2}{\omega_m(\mathbf{q}_\parallel)} \times \sin^2\left(\frac{aq_{t,m}}{2}\right)\mathscr{G}(q_{l,m}), \tag{6}$$

$\delta(x)$ is the delta function, $n_{\mathbf{q}_\parallel,m}$ is the phonon occupation number, $\varepsilon=\hbar^2k_\parallel^2/2m^*$ and $\varepsilon'=\hbar^2k'^2_\parallel/2m^*$ are the electron energies before and after scattering, m^* is the electron effective mass. Throught this paper the upper signs correspond to the phonon absorption, the lower signs correspond to the phonon emission. The overlap integral, $\mathscr{G}(q)$, is given by the formula

$$\mathscr{G}(q)=\left|\int_{-a/2}^{a/2}dz\,\psi^*(z)\psi(z)\cos(qz)\right|^2,$$

where $\psi(z)$ is the ground state solution of the one dimensional Schrödinger equation. The argument q takes both real and pure imaginary values. If we use the electron wave functions for a rectangular infinitely deep quantum well, the overlap integral takes the form

$$\mathscr{G}(q)=\frac{32(1-\cos\pi\tilde{q})}{\pi^2(\tilde{q}^2-4)}$$

where $\tilde{q}=aq/\pi$, and q is a real or a pure imaginary number.

To analyze the electron transport properties we will need scattering rates in the following form

$$\tau_G^{-1}=\sum_{\mathbf{k}'_\parallel,m,\mathbf{q}_\parallel,\beta}W^\beta_{\mathbf{k}_\parallel\to\mathbf{k}'_\parallel}G, \tag{7}$$

where β is used to denote either *absorption* or *emission*, G is some given function which may depend on all variables over which we take the sum. We will also use $(\tau_G^{ab})^{-1}$ and $(\tau_G^{em})^{-1}$ which are defined in a similar way with the only distinction that we sum either only absorption terms or only emission terms. There is an obvious relation between them: $\tau_G^{-1}=(\tau_G^{ab})^{-1}+(\tau_G^{em})^{-1}$. If we employ the formulae for transition probabilities (5) we may obtain the following result for the scattering rates

$$\left(\tau_G^{\{ab\}_{em}}\right)^{-1}=\frac{E_a^2m}{2\pi\hbar^2\rho k_\parallel}\sum_m\int_0^\infty dq_\parallel\mathscr{F}^{\{ab\}}_{\{em\}}(m,q_\parallel)G\frac{1}{|\sin\Psi|}, \tag{8}$$

and the angle $\Psi\in[0,\pi]$ is a solution of the transcendental equation

$$\cos\Psi=\frac{m\omega_m(q_\parallel)}{\hbar k_\parallel q_\parallel}\mp\frac{q_\parallel}{2k_\parallel}.$$

Actually, the angle Ψ is the angle between $\mathbf{k}_\parallel$ and $\mathbf{q}_\parallel$. In the transition from Eq. (7) to Eq. (8) we have replaced the summation over a quasidiscrete variable by integration in accordance with the rule $\Sigma_{\mathbf{k}_\parallel}=(\mathscr{A}/2\pi^2)\int d\mathbf{k}_\parallel$. Hereinafter we will use summation and integration over quasidiscrete variables interchangeably for the sake of convenience.

The deformation potential which we have considered above is the major mechanism of electron–acoustic phonon interactions in FSQWs. The Hamiltonian for it in FSQWs has been obtained in Ref. 12. The ratio of the piezoelectric potential strength to the deformation potential strength is equal to $(ee_{14}/E_aq)^2$, where e_{14} is the piezoelectric constant and q is the wave vector of the participating in the scattering phonon. In bulk semiconductors the piezoelectric scattering becomes stronger than the deformation potential scattering at low lattice temperatures and in low electric fields because electrons are scattered mainly by acoustic phonons with small q. In FSQWs there is a lower limit for q which is equal to π/a due to the q_z component quantization. For this reason the deformation potential scattering dominates in FSQWs.

III. MOMENTUM RELAXATION TIME

We have solved the electron transport problem for FSQW in the linear in respect to the drawing electric field approximation assuming that the electron scattering by confined acoustic phonons through the deformation potential is dominant. The electron distribution function (DF) $f=f(\mathbf{p})$ ($\mathbf{p}$ is the electron momentum) may be represented in the form

$$f=f_p^0+\frac{\mathbf{f}_{1p}\mathbf{p}}{p}, \tag{9}$$

where functions f_p^0 and $\mathbf{f}_{1p}$ depend on the absolute value of $\mathbf{p}$ and do not depend on its direction. The first term in the Eq. (9) is the symmetric part of DF and the second term is the antisymmetric part of DF. Because we are looking for the linear transport properties (formally the external force $F\to 0$) the symmetric part of DF is the equilibrium Fermi function. DF satisfies the standard kinetic equation (see e.g. Ref. 20) with electron–confined acoustic phonon collision integral. We multiply the kinetic equation for DF defined by Eq. (9) by factor $\mathbf{p}/p$ and average it over the polar angle ϕ [vector $\mathbf{p}$ has components (p,ϕ) in the polar coordinate system]. In the end we get the following equation for the antisymmetric part of DF

$$\mathbf{F}\frac{\partial f_p^0}{\partial p}=\sum_{\mathbf{p}'} W_{\mathbf{p}\to\mathbf{p}'}\left(\frac{f_p^0}{f_{p'}^0}\mathbf{f}_{1p'}\cos\varphi-\frac{1-f_{p'}^0}{1-f_p^0}\mathbf{f}_{1p}\right), \tag{10}$$

where $\mathbf{F}$ is the external force, $W_{\mathbf{p}\to\mathbf{p}'}$ is the electron transition probability density defined by Eq. (5), φ is the angle between $\mathbf{p}$ and $\mathbf{p}'$. We are looking for the solution of Eq. (10) in the following form

$$\mathbf{f}_{1p}=-\tau_1(p)\mathbf{F}\frac{\partial f_p^0}{\partial p}. \tag{11}$$

Eq. (11) redefines the unknown function $\mathbf{f}_{1p}$ through the function $\tau_1(p)$. It will be shown below that $\tau_1(p)$ may be interpreted as the electron momentum relaxation time. From Eqs. (10), (11) we may obtain the Fredholm equation of the second kind for the function $\tau_1(p)$

$$\tau_1(p)=\tau(p)+\tau(p)\sum_{\mathbf{p}'} W_{\mathbf{p}\to\mathbf{p}'}\frac{p'\cos\varphi}{p}\tau_1(p')\frac{1-f_{p'}^0}{1-f_p^0}, \tag{12}$$

where

$$\tau(p)^{-1}=\sum_{\mathbf{p}'} W_{\mathbf{p}\to\mathbf{p}'}\frac{1-f_{p'}^0}{1-f_p^0}. \tag{13}$$

Eq. (12) may be transformed to the following mathematically equivalent equation

$$\tau_1(p)^{-1}=\sum_{\mathbf{p}'} W_{\mathbf{p}\to\mathbf{p}'}\left(1-\frac{p'\cos\varphi}{p}\frac{\tau_1(p')}{\tau_1(p)}\right)\frac{1-f_{p'}^0}{1-f_p^0}. \tag{14}$$

It is worth noting that Eq. (14) differs from the equation for the momentum relaxation time, $\tau_p(p)$, in the test particle approximation (TPA) which was obtained and analyzed in Ref. 14 only by the factor $\tau_1(p')/\tau_1(p)$. Accordingly, the equation for $\tau_p(p)$ has the following form

$$\tau_p(p)^{-1}=\sum_{\mathbf{p}'} W_{\mathbf{p}\to\mathbf{p}'}\left(1-\frac{p'\cos\varphi}{p}\right)\frac{1-f_{p'}^0}{1-f_p^0}. \tag{15}$$

To transform the sum in Eqs. (12), (14), and (15) to the integral and to include the explicit expression for the electron transition probability density due to scatterings by confined acoustic phonons we used the result obtained in the previous section and expressed by the formulae (7) and (8). Variational methods were almost exclusively employed until recently to numerically solve Eqs. (12) or (14).[21] We have solved Eqs. (12) and (14) numerically using iterative procedures. The unknown function from the previous iteration has been used in the right hand side to obtain the updated function. The function $\tau_p(p)$ has been used as an initial guess. Although Eqs. (12) and (14) are equivalent mathematically, they are not equivalent from the computational point of view. Our iterative procedure had faster convergence if applied to Eq. (14) than to Eq. (12). However results were the same within the accepted computational accuracy, which was taken to be equal to 0.1% in the relative error. The iterative method converges fast in the case of a nondegenerate electron gas and in the case of a degenerate electron gas and high lattice temperatures ($T>10$ K). It took many more iterations (on the average, about 100) to obtain the convergence of the solution if the electron gas is degenerate and the lattice temperature is low ($T<5$ K). This transitional temperature corresponds to the characteristical energy of the acoustic phonon quantization. The numerical analysis was done for GaAs FSQW of width $a=100$ Å We took into account five of the lowest phonon modes; modes of the higher order make unnoticeable contribution to the scattering rate.

The inverse momentum relaxation time, τ_1^{-1}, obtained by solving Eq. (14), and the inverse momentum relaxation time in TPA, τ_p^{-1}, for nondegenerate electron gases at three different temperatures are shown in Fig. 2. The comparison of τ_1^{-1} and τ_p^{-1} in a wide range of electron temperatures demonstrates that the test particle approximation is quite accurate in the case of a nondegenerate electron gas. However even in this case there is a fine structure in the energy dependence of τ_1^{-1} which is more pronounced in the case of low lattice temperature. Before we discuss the origination of this structure we would like to note a very important property of the solution τ_1^{-1}. Eqs. (12) and (14) are linear in respect to unknown function τ_1 [Eq. (14) has a nonlinear form because it is an equation for τ_1^{-1}]. However these equations are nonlinear in respect to different terms in the representation of $W_{\mathbf{p}\to\mathbf{p}'}$, which includes the sum of emission terms and absorption terms for several (five in our case) dilatational modes. Accordingly, the Matthiessen rule is not applicable and the momentum relaxation time, τ_1^{-1}, may not be represented as a sum of terms corresponding to the individual types of scatterings. It was possible in the case of the similar function τ_p^{-1} in TPA, because the equation for it does not contain the unknown function in the right hand side.

It is seen from the graph for function τ_p^{-1}, that the first dilatational mode makes the main contribution to the electron scattering (it corresponds to the steep step at 1.2 meV in Fig. 2), the zeroth and the second modes are also noticeable in Fig. 2 (steps at electron energies 0 meV and 1.4 meV correspondingly), the modes of the higher order make contributions which are smaller than the resolution of the graphs. Some decrease in the function τ_1^{-1} at energies

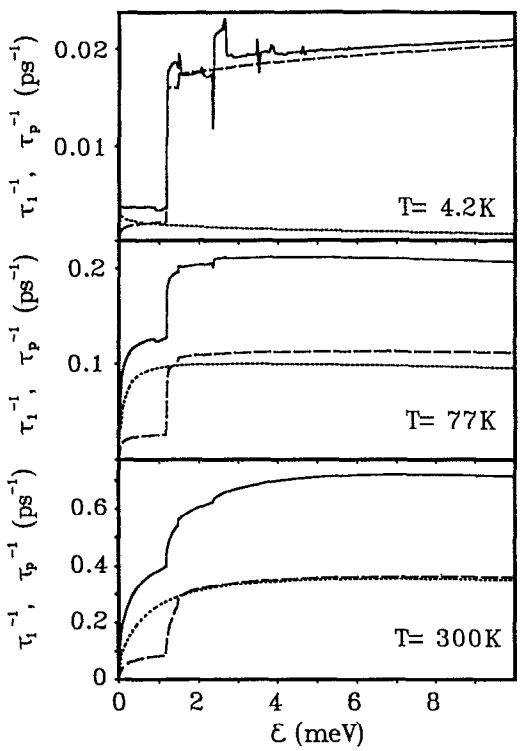

FIG. 2. The inverse momentum relaxation time, τ_1^{-1} (solid line), and the inverse momentum relaxation time in the test particle approximation, τ_p^{-1} (dashed line corresponds to phonon emission and dotted line corresponds to phonon absorption), as functions of electron energy for nondegenerate electron gas in GaAs FSQW of width $a=100$ Å for $T=4.2$ K, $T=77$ K, and $T=300$ K.

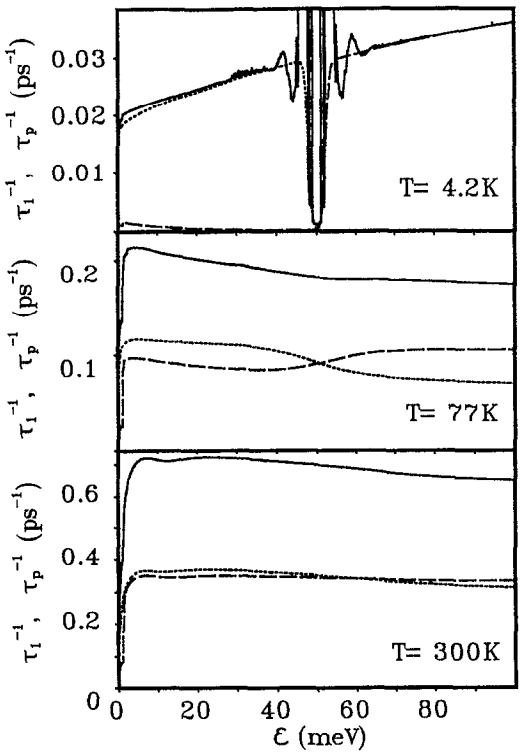

FIG. 3. The inverse momentum relaxation time, τ_1^{-1} (solid line), and the inverse momentum relaxation time in the test particle approximation, τ_p^{-1} (dashed line corresponds to phonon emission and dotted line corresponds to phonon absorption), as functions of electron energy for degenerate electron gas in GaAs FSQW of width $a=100$ Å for $T=4.2$ K, $T=77$ K, and $T=300$ K; $\varepsilon_F=50$ meV.

just lower that 1.2 meV and an increase at energies just higher that 1.2 meV in respect to the energy dependence of τ_p^{-1} is related to the steep variation of the ratio $\tau_1(p')/\tau_1(p)$ near the threshold energy of the first dilatational phonon. An additional structure in the energy dependence of τ_1^{-1} at 2.4 meV is a translation of the similar dependence at 1.2 meV to the region of higher energy. It is due to the fact that electrons with energy about 2.4 meV may emit phonons of the first dilatational mode with energies in the range $1.1-1.3$ meV which have very high density of states (see Fig. 1) and get the final energy near the threshold for the first dilatational mode, so the ratio $\tau_1(p')/\tau_1(p)$ in the Eq. (14) will be very sensitive to the initial electron energy. The modes of the zeroth and the second order make their own contribution to the energy dependence of τ_1^{-1} which, as it was discussed above, may not be separated and the overall behavior of τ_1^{-1} is quite complex.

We have performed calculations of the inverse momentum relaxation times, τ_1^{-1} and τ_p^{-1}, in the case of a degenerate electron gas in a wide range of the lattice temperatures. The Fermi energy is taken to be equal to $\varepsilon_F=50$ meV, which corresponds to the electron concentration 1.4×10^{12} cm^{-2}. The results of our calculations for $T=4.2$ K, $T=77$ K, and $T=300$ K are displayed in Fig. 3. Similarly to the case of a nondegenerate electron gas the energy dependences of τ_1^{-1} and τ_p^{-1} are very close to each other if the lattice temperature is high. If the lattice temperature is lower than the energy of the first dilatational mode (about 1 meV$\approx$ 10 K), the inverse momentum relaxation time, τ_1^{-1}, acquires a highly pronounced additional structure at energies near the Fermi energy. We have studied this effect in more detail calculating the unknown function, τ_1^{-1}, on a very fine mesh in the two-dimensional space *electron energy –lattice temperature*. The overall behavior of τ_1^{-1} is shown on the three-dimensional graph in Fig. 4 in the temperature range 3 K–5 K. More detailed energy dependencies for τ_1^{-1} are demonstrated in Fig. 5.

The obtained functions for τ_1^{-1} are almost symmetrical in respect to ε_F in an energy range near the Fermi level. There are two symmetrical peaks at energies $\varepsilon_F\pm1.3$ meV which disappear at the lattice temperature $T=4.47$ K . There are also two other peaks wider than those mentioned above and located approximately at energies $\varepsilon_F\pm3.5$ meV. These peaks have some substructures which also disappear at the lattice temperature $T=4.47$ K. Although the peaks themselves are being preserved, they become smoother and smaller and disappear at a lattice temperature higher than 10 K. On the contrary the peaks located closer to the Fermi level maintain their magnitude and position until disappearance at $T=4.47$ K. When the lattice temperature approaches $T=4.47$ K these peaks become thinner and thinner and finally disappear at $T=4.47$ K.

The approximate symmetry of τ_1^{-1} in respect to the Fermi energy $\varepsilon_F=50$ meV follows from the analysis of the

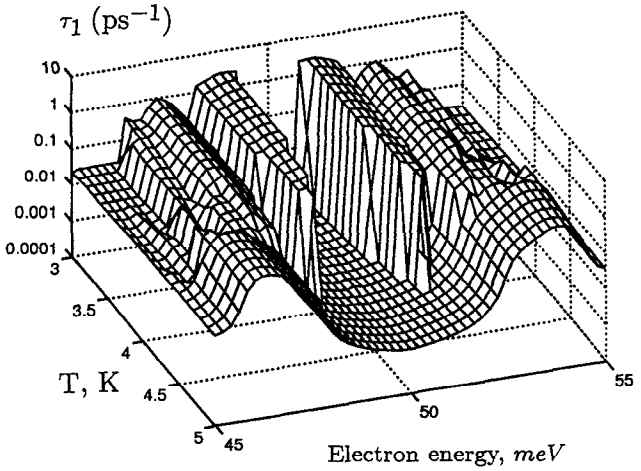

FIG. 4. The inverse momentum relaxation time, τ_1^{-1}, as a function of the electron energy and the lattice temperature. GaAs FSQW of width $a=100$ Å, $\varepsilon_F=50$ meV.

integrand in Eq. (14). The quantum mechanical probability is the same for both transitions: for phonon emission ($\mathbf{k}_\parallel'=\mathbf{k}_\parallel+\mathbf{q}_\parallel$) and for phonon absorption ($\mathbf{k}_\parallel+\mathbf{q}_\parallel=\mathbf{k}_\parallel'$) as long as the same quantum states $\mathbf{k}_\parallel,\mathbf{k}_\parallel',\mathbf{q}_\parallel$ are involved. There is an additional factor in Eq. (14) which is symmetrical in respect to the Fermi energy, ε_F, and it makes a decisive impact on the symmetry of the momentum relaxation time. It reflects the population of the electron and phonon states. For the case of the phonon absorption we denote it as $\mathscr{P}_a(\varepsilon)$ and for the case of the phonon emission we denote it as $\mathscr{P}_e(\varepsilon)$. In accordance with Eqs. (5), (6), (14)

$$\mathscr{P}_a(\varepsilon)=n_{\hbar\omega}\frac{1-f^0_{\varepsilon+\hbar\omega}}{1-f^0_\varepsilon},\quad \mathscr{P}_e(\varepsilon)=(n_{\hbar\omega}+1)\frac{1-f^0_{\varepsilon-\hbar\omega}}{1-f^0_\varepsilon}.$$

Subscripts in the above equations denote the appropriate energies. It may be easily shown that

$$\mathscr{P}_a(\varepsilon_F\pm\varepsilon)=\mathscr{P}_e(\varepsilon_F\mp\varepsilon).$$

Thus, the electron in quantum state $\mathbf{k}_\parallel'$ emits the phonon in quantum state $\mathbf{q}_\parallel$ and acquires the final state $\mathbf{k}_\parallel$ with exactly the same probability as probability of the opposite process: electron in quantum state $\mathbf{k}_\parallel$ absorbs phonon in quantum state $\mathbf{q}_\parallel$ and acquires the final state $\mathbf{k}_\parallel'$. Actually this is nothing more than the principle of the detailed balance. It ensures that the discussed symmetry of the momentum relaxation time to be preserved.

It is obvious that the origin of the peaks stems from the electron scattering by acoustic phonons whose energy is quantized. It follows from the analysis of $\mathscr{P}_a(\varepsilon)$ and $\mathscr{P}_a(\varepsilon)$ that if the lattice temperature, T, is lower than the phonon energy, $\hbar\omega$, then the electrons with energies $\varepsilon>\varepsilon_F+\hbar\omega$ primarily emit phonons [emission is in $\exp(\hbar\omega/T)$ times more probable than absorption], electrons with energies $\varepsilon<\varepsilon_F-\hbar\omega$ primarily absorb phonons [absorption is in $\exp(\hbar\omega/T)$ times more probable than emission]. Accordingly, the peaks in the energy dependence of τ_1^{-1} are associated with phonon emission (on the right of the Fermi energy) and phonon absorption (on the left of the Fermi

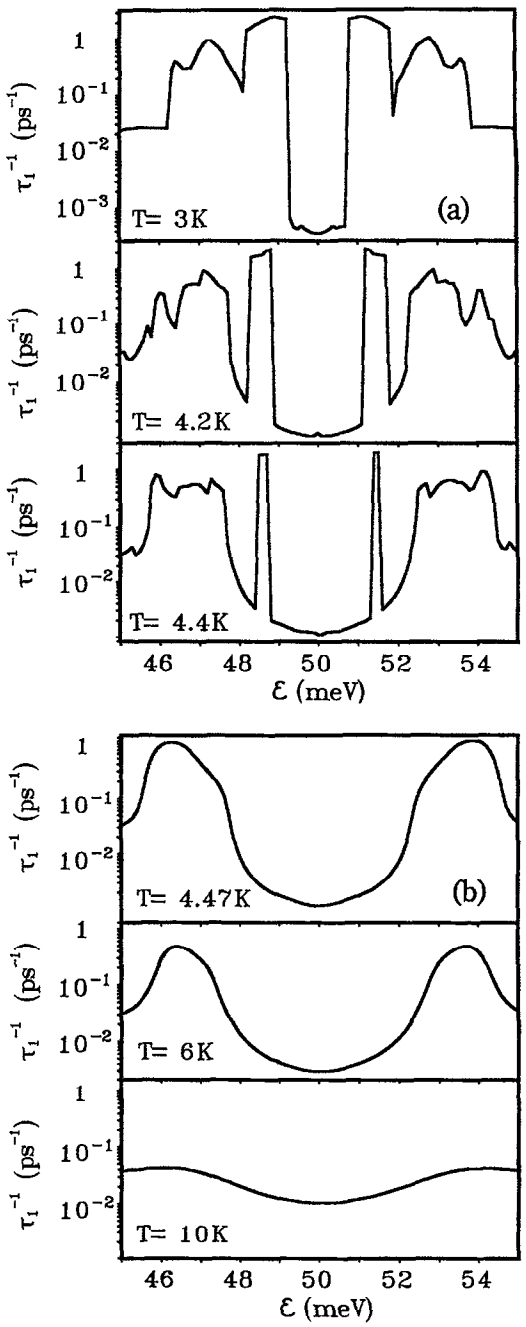

FIG. 5. The inverse momentum relaxation time, τ_1^{-1}, as a function of the electron energy for lattice temperatures $T=3$ K, $T=4.2$ K, $T=4.4$ K (a), and $T=4.47$ K, $T=6$ K, $T=10$ K (b). *GaAs* FSQW of width $a=100$ Å, $\varepsilon_F=50$ meV.

energy). The maximum acoustic phonon wave vector is approximately equal to doubled k_F and in our case constitutes 6×10^6 cm^{-1}. If we restrict the length of the wave vector by this maximum value, the energies of five the lowest mode acoustic phonons lies in the ranges (see Fig. 1) 0–1.3 meV, 1.1–2.2 meV, 1.3–2.5 meV, 2.4–3.2 meV, 3.5–4.0 meV. Due to interference of different phonon modes, the positions of the peaks in τ_1 and consequently in the antisymmetric part of the distribution function are determined by a simultaneous action of all the

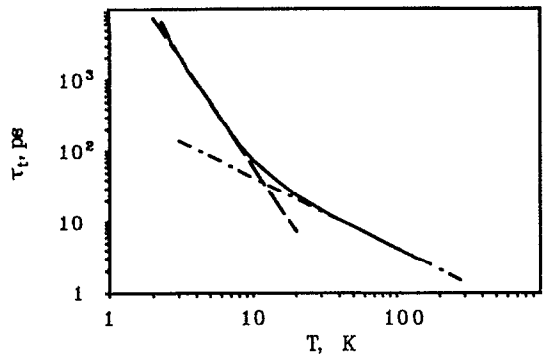

FIG. 6. The transport relaxation time, τ_t (solid line), as a function of the lattice temperature. The dotted line corresponds to the dependence $1/T$, the dashed line corresponds to the dependence $1/T^3$. Transition to the Bloch-Grüneisen regime occurs in the temperature range 40 K– 8 K. GaAs FSQW of width $a=$ 100 Å, $\varepsilon_F=50$ meV.

confined modes. Mathematically it is expressed in the nonlinearity of Eq. (14) in respect to scatterings by different phonon modes which is discussed above. The lattice temperature at which two peaks near the Fermi energy cease to exist (4.47 K) corresponds to the characteristic energy of the acoustic phonon quantization.

IV. LOW FIELD ELECTRON MOBILITY

The electron mobility, μ, is expressed by the formula $\mu=e\tau_t/m^*$, where τ_t is the transport relaxation time obtained by averaging τ_1:

$$\tau_t=\frac{\int_0^\infty d\varepsilon(\varepsilon/T)\tau_1(\varepsilon)f_p^0(1-f_p^0)}{\int_0^\infty d\varepsilon f_p^0}. \tag{16}$$

We took integral (16) for series of temperatures and obtained temperature dependences of τ_t and electron mobility. We will consider here only the case of a degenerate electron gas ($\varepsilon_F=$ 50 meV). The temperature dependence of τ_t is shown in the Fig. 6. This result is very similar to the temperature dependence of μ for the 2DEG in GaAs$-$Al$_x$Ga$_{1-x}$As heterostructure observed in Ref. 22. At high lattice temperatures the phonon population is much larger than unity and proportional to the lattice temperature. Therefore the rate of the electron scattering by phonons and the electrical resistivity are proportional to the lattice temperature. At low lattice temperatures the phonon occupation number is less than unity for substantial part of phonons and consequently their contribution to the electron scattering is significantly reduced. In the case of metals this results in T^{-5} dependence of the electron mobility (Bloch-Grüneisen formula[21]). The same power dependence has been observed for 2DEG semiconductor quantum well.[22] We have obtained a smaller negative power (T^{-3}) for the temperature region (3 K$<T<$ 8 K). This results in a smaller τ_t and electron mobility than in the case of a double barrier heterostructure. For lattice temperatures $T<$ 3 K the negative power becomes larger (see Fig. 6), however we did not proceed with our calculations below $T<$ 2 K because the convergence of our computational algorithm deteriorates when the lattice temperature decreases.

A peculiarity of the Bloch-Grüneisen regime (the temperature range in which the electron-phonon scattering processes are dominated by restraining $k-$space selection rules[22]) in FSQWs consists in a discrete character of transition from linear region to nonlinear region. In FSQWs electrons are scattered by several acoustic modes which have consecutively growing frequencies. If we decrease the lattice temperature, the most energetic mode will cease to be thermally exited first, then the next in energy mode will be frozen out, and so on. The lowest mode begins loosing thermally exited states with large in-plane wave vectors at $T=$ 10 K. The transition from the linear dependence of τ_1 to Bloch-Grüneisen regime takes place in the temperature range 40 K–8 K.

It is interesting to note that though the momentum relaxation rate τ_1^{-1} has peaks near the Fermi energy, the transport relaxation time, τ_t, and the electron mobility, μ, do not have peaks associated with quantized acoustic phonons. Such peaks have been observed in the conduction variations of the electrically heated AuPd films and wires.[11] However their origination lies in the nonlinear response of the electron – phonon system on the heating electric field. A similar dependence could be observed in the energy loss due to emission of the acoustic phonons.

V. SUMMARY AND CONCLUSIONS

We have solved the kinetic equation for 2DEG in FSQW for the case where only the first electron subband is occupied in the low drawing electric field limit. We have considered both nondegenerate and degenerate electron gases in a wide range of lattice temperatures. The dominant mechanism of the electron scattering is taken to be the deformation potential interactions with several of the lowest mode dilatational phonons. We obtained the electron momentum relaxation time τ_1 and the electron mobility. In the case of a degenerate electron gas τ_1^{-1} has several peaks at low temperatures related to the interactions with different quantized phonons. The electron mobility has the lattice temperature dependence which is similar to the Bloch-Grüneisen formula. It has T^{-1} dependence at a high lattice temperatures and T^{-3} dependence at low lattice temperatures. The transition temperature is not clearly pronounced and the transition occurs in the temperature range 40 K–8 K.

Our calculations are based on a model of FSQW with perfect parallel surfaces. Real structures have finite roughness which may affect measurable quantities. The closest to ideal FSQWs are unsupported metal films. The Brillouin light scattering from such films gives confined phonon spectra which are very close to the theoretical predictions.[6] Semiconductor FSQWs are less perfect.[1] The rough surfaces cause modification of both electron and phonon states which will depend on statistical properties of the spatial fluctuations. Electron transport in such systems is much more complicated and we will only outline its qualitative features. Rough surfaces may be treated as an additional source of scattering for both phonons and electrons. If the thickness of the FSQW is *very small*, surface scattering may significantly reduce electron mobility.[23] The effect of the surfaces rough-

ness on the relaxation times, which we have calculated, consists in smearing of fine structures as well as in smoothing a transition from the linear regime to the Bloch-Grüneisen regime. It occurs because the energy of confined phonons is inversely proportional to the FSQW thickness which fluctuates; at the same time, positions of the peaks depend on the phonon energy. The two regimes of conductivity are the consequence of the restrictions in k–space for degenerate systems at low temperatures, therefore they will exist in FSQWs with rough surfaces. The last effect which we would like to mention consists in a possible localization of acoustic phonon modes in FSQWs with rough surfaces. It is similar to photon localization[24] or electron localization in low-dimensional systems.

ACKNOWLEDGMENTS

This work was supported by NSF and ARO.

[1] A. K. Viswanath, K. Hiruma, M. Yazawa, K. Ogawa, and T. Katsuyama, Microw. Opt. Techn. Lett. **7**, 94 (1994).
[2] K. Yoh, A. Nishida, H. Kunitomo, T. Ogura, and M. Inoue, Jpn. J. Appl. Phys. (Pt. 1) **32**, 6237 (1993).
[3] K. Hiruma, M. Yazawa, K. Haraguchi, K. Ogawa, T. Katsuyama, M. Koguchi, and H. Kakibayashi, J. Appl. Phys. **74**, 3162 (1993).
[4] M. A. Foad, C. D. Wilkinson, C. Dunscomb, and R. H. Williams, Appl. Phys. Lett. **60**, 2531 (1992).
[5] K. Tsutsui, E. L. Hu, and C. Wilkinson, Jpn. J. Appl. Phys. (Pt. 1) **32**, 6233 (1993).
[6] B. Bhadra, M. Grimsditch, I. Schuller, and F. Nizzoli, Phys. Rev. B **39**, 12 456 (1989).
[7] M. D. Williams, S. C. Shunk, M. G. Young, D. P. Docter, D. M. Tennant, and B. I. Miller, Appl. Phys. Lett. **61**, 1353 (1992).
[8] T. Itoh and T. Suga, Jpn. J. Appl. Phys. (Pt. 1) **33**, 334 (1994).
[9] S. T. Ho, S. L. McCall, R. E. Slusher, L. N. Pheiffer, K. W. West, A. Levi, G. Blonder, and J. Jewell, Appl. Phys. Lett. **57**, 1387 (1990).
[10] T. S. Ravi and R. B. Marcus, J. Vac. Sci. Technol. B **9**, 2733 (1991).
[11] J. Seyler and M. N. Wybourne, Phys. Rev. Lett. **69**, 1427 (1992).
[12] N. Bannov, V. Mitin, and M. Stroscio, Physica Status Solidi B **183**, 131 (1994).
[13] N. Bannov, V. Aristov, and V. Mitin, Solid State Commun. **93**, 483 (1995).
[14] N. Bannov, V. Aristov, V. Mitin, and M. A. Stroscio, Phys. Rev. B **51**, 9930 (1995).
[15] S. Yu, K. W. Kim, M. A. Stroscio, G. Iafrate, and A. Ballato, Phys. Rev. B **50**, 1733 (1994).
[16] M. A. Stroscio and K. W. Kim, Phys. Rev. B **48**, 1936 (1993).
[17] N. Nishiguchi, Jpn. J. Appl. Phys. **33**, 2852 (1994).
[18] K. Johnson, M. N. Wybourne, and N. Perrin, Phys. Rev. B **50**, 2035 (1994).
[19] B. A. Auld, *Acoustic Fields and Waves in Solids,* Vol. 2 (Krieger, Malabar, 1990).
[20] D. K. Ferry, *Semiconductors* (Macmillan, New York, 1991).
[21] G. Grimvall, *The Electron–Phonon Interactions in Metals* (North-Holland, Amsterdam, 1981).
[22] H. L. Stormer, L. N. Pfeiffer, K. W. Balwin, and K. W. West, Phys. Rev. B **41**, 1278 (1990).
[23] H. Sakaki, T. Noda, K. Hirakawa, M. Tanaka, and T. Matsusue, Appl. Phys. Lett. **51**, 1934 (1987).
[24] T. Nakayama, K. Yakubo, and M. Takano, Phys. Rev. B **47**, 9249 (1993).